SURFACE AND INTERFACE ANALYSIS
Surf. Interface Anal. 2002; **33**: 185–195
Published online in Wiley InterScience (www.interscience.wiley.com). DOI: 10.1002/sia.1201

SIA

Multivariate image analysis methods applied to XPS imaging data sets

Kateryna Artyushkova and Julia E. Fulghum*

Chemistry Department, Kent State University, Kent, OH 44242, USA

Received 12 July 2001; Revised 14 December 2001; Accepted 14 December 2001

Recent improvements in imaging photoelectron spectroscopy enhance lateral and vertical characterization of heterogeneous samples at the cost of increasing complexity in the XPS data sets acquired. These imaging data sets require more sophisticated analysis methods than visual inspection if the data are to be interpreted effectively. Multivariate analysis (MVA) methods are increasingly utilized in surface spectroscopies to aid the analyst in interpreting the vast amount of information resulting from these multidimensional data set acquisitions.

In this work, image processing analysis methods are tested on XPS data sets acquired from polymer blends. Images from the blends, acquired as a function of composition, time or energy, provide multidimensional data sets for algorithm evaluation. Multivariate image analysis (MIA) methods such as scatter diagrams, principal component analysis (PCA) and classification methods are used to extract maps of pure components from degradation and images-to-spectra data sets. In some cases the MVA results can be compared directly with the XPS spectra or images, which provide a critical reference point. This work will demonstrate that additional information can result from the application of MIA methods, even when direct spectral or image interpretation is possible. Copyright © 2002 John Wiley & Sons, Ltd.

KEYWORDS: surface analysis; XPS; multivariate image analysis; MIA; scatter plot; PCA; classification; polymer blends

INTRODUCTION

Recent advances in XPS instrumentation enhance lateral and vertical characterization of heterogeneous samples, at the cost of increasing complexity in the data sets that are acquired. Multidimensional data sets quickly follow the development of imaging capabilities in an analytical technique. In an XPS images-to-spectra experiment, for example, images are acquired as a function of binding energy. The intensities from a single pixel or groups of pixels then can be plotted as a function of energy, providing spectra from smaller areas than is possible using more traditional spectroscopic acquisitions. The resulting multispectral imaging data sets are a complex data structure that requires more sophisticated analysis methods than visual inspection if the data are to be interpreted effectively.[1] Appropriate methods for multispectral image analysis of complex imaging data sets have been developed for Earth satellite image processing and are directly applicable to surface microanalysis.[2,3] Multivariate analysis (MVA) methods increasingly are being utilized in surface spectroscopies to aid the analyst in interpreting the vast amount of information resulting from multidimensional data set acquisitions.

Although the application of MVA methods to surface analysis data is increasing, there has been no systematic comparison of the numerous approaches available for the analysis of multidimensional data. This comparison has been made in the areas of separation science and near-infrared spectroscopy but the conclusions are not applicable directly due to the differences in signal/noise and data structure.[4–7] Multivariate analysis methods have been used in the analysis of surface science data by several groups. The application of scatter diagrams, as well as factor and principal component analysis, has been illustrated for the surface analysis of semiconducting, catalytic and magnetic structures for MULSAM instrumentation.[8,9] Several groups have used classification and scatter diagrams for time-of-flight secondary ion mass spectrometry (ToF-SIMS) depth profile analysis.[10,11] Some of the applications of MVA methods to surface analysis data have been limited to the use of software provided by the instrument manufacturers. The software for MVA methods, neural nets and other classification methods is now readily available, however, and most instruments produce spectra and images in a format that can be ported readily into independent software. It has, thus, only recently become possible to evaluate fully the application of MVA and classification methods to surface analysis data.

*Correspondence to: J. E. Fulghum, Chemistry Department, Kent State University, Kent, OH 44242, USA.
E-mail: jfulghum@lci.kent.edu
Contract/grant sponsor: NSF ALCOM; Contract/grant number: DMR89-20147.
Contract/grant sponsor: Keck Foundation.
Contract/grant sponsor: NSF; Contract/grant number: CHE-9613880.

X-ray photoelectron spectroscopy data sets are generally less complex than the hyperspectral data sets that can be obtained using ToF-SIMS or Fourier transform infrared (FTIR), making them useful for an evaluation of MVA methods. In this work, we use XPS data from a heterogeneous polymer blend in the evaluation of results from a variety of MVA approaches. Multivariate methods are tested by comparing the extracted information (number and identification of components) with the chemical information obtained directly from the XPS data. Direct comparison of the MVA results to the spectra or images provides a critical reference point. A multispectral images-to-spectra data set and images acquired from poly(vinyl chloride) (PVC)/poly(methyl methacrylate) (PMMA) blends as a function of x-ray exposure time provide the multidimensional data sets for algorithm evaluation. The PVC degrades upon prolonged exposure to the x-ray beam through a dehydrohalogenation process in which carbon–chlorine bonds are replaced by double bonds, with a release of hydrogen chloride. The PVC degradation thus results in changes in peak intensities and positions in both survey and high-resolution spectra, affecting image appearance.[12–14]

THEORY BEHIND MULTIVARIATE IMAGE ANALYSIS

Multivariate analysis has been explained in a number of sources.[15–20] The data types and analysis methods used in this comparison are briefly described below. All of the methods discussed can be implemented using commercially available software, as listed in the Experimental section.

Imaging data set types

The simplest imaging data type is a single image, resulting from acquisition of a map of a specific elemental or chemical state distribution. For multicomponent samples, several images from the same area of a specimen frequently are acquired. A static series, composed of several different images or maps of different elemental or chemical states, results in a bivariate data set. Multispectral data sets contain a series of images acquired as a function of, for example, the binding energy for XPS, the m/z for ToF-SIMS or the wavelength for FTIR. Finally, multitemporal data sets consist of a dynamic series in which the elemental or chemical content is studied as a function of an external parameter, which can be a space coordinate (depth profiling), time (time-resolved imaging), temperature, etc.

Multivariate imaging analysis methods

Scatter diagrams

Elemental or chemical variations in images lead to pixel populations in coherent clusters. To identify different features in the image space, the frequency distribution of these populations is determined. The histogram of the digital image is a plot or graph of the frequency of occurrence of each grey level (pixel intensity) in the image. A scatter diagram, or two-dimensional histogram, yields information about the intensity relationships between two or more elemental or chemical maps, leading to the calculation of chemical phase maps.[15,16] Scatter diagrams can be used to display simultaneously the information in bivariate data sets containing two elemental or chemical maps. The scatter diagram results in groupings of points that reflect different classes of pixels present in the two images. This approach provides a rapid analysis of image content in terms of correlation (points along the first diagonal) and anti-correlation (clusters of points along the second diagonal). If a cluster of representative points, or part of a cluster, in a scatter diagram is selected, the group of points can be back-projected to the regions of the image that contribute to the cluster. After the back-projection, the spatial relationship of pixels possessing a chemical similarity can be studied. This method is sometimes called *interactive correlation partitioning* (ICP). The basis of the scatter plot and ICP is illustrated in Plate 1 for two simulated images.

Principal component analysis

It is difficult to evaluate more than three images with scatter diagrams or ICP. Larger image data sets can be analyzed using multivariate image analysis (MIA). The goal of MIA methods is to extract significant information from an image data set while reducing the dimensionality of the data.[17,18] Principal component analysis (PCA) divides information into orthogonal components by transforming multivariate images into a number of factorial (also called latent or principal component or *score*) images that carry information related to these orthogonal components. The first principal component accounts for as much of the variability in the data as possible and has the largest eigenvalue, λ, associated with it, and each succeeding component accounts for as much of the remaining variability as possible. The primary components are those corresponding to the largest r eigenvalues and represent the set of r components that are required to reproduce the original data within experimental error. The remaining factors, each describing a low variance, represent the noise in the data set. The idea behind PCA is presented in Fig. 1. The objective is to identify images that are globally correlated or anti-correlated. This information can be displayed as *loadings* of the different maps, whereas the pixels that are responsible for the correlations can be displayed as component images. Component images may be easier to interpret than pure

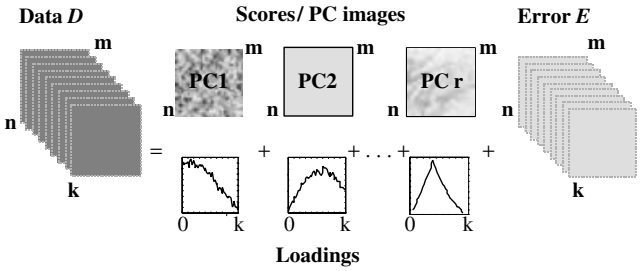

Figure 1. Introduction into the Image Principal Component Analysis algorithm. A series of k images is decomposed via PCA into r principal component images (score images) and loadings associated with each principal component image. The r components represent significant variation within the original data set D, whereas $(k - r)$ components represent noise in the data and are included into error E.

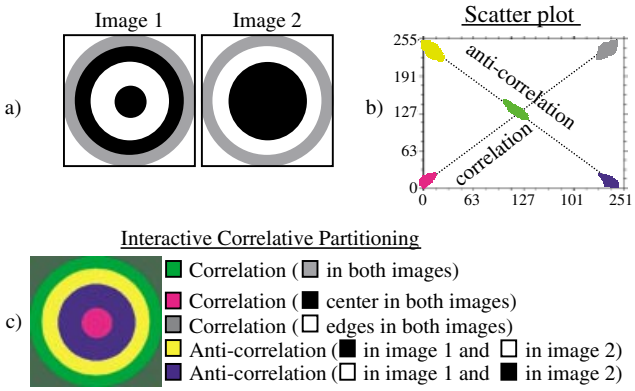

Plate 1. Scatter plot and interactive correlative partitioning: (a) two original images; (b) scatter plot; (c) back-projected areas from the scatter plot to the original image. The scatter plot results in five clouds representing different parts of images in terms of their correlation and anticorrelation. Five phases are back-projected to the original image.

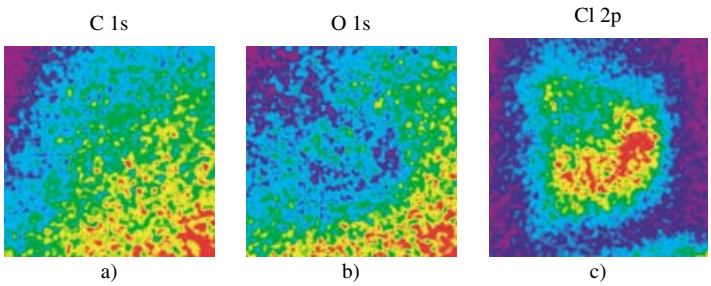

Plate 2. Photoelectron C 1s (a), O 1s (b) and Cl 2p (c) images acquired from the same area on the sample. The C 1s image is a homogeneous, featureless image to which both polymers contribute. Bright areas in the O 1s image are enriched in PMMA, whereas bright areas in the Cl 2p image are enriched in PVC. Note an anti-correlation between the O 1s and Cl 2p images, indicating phase separation between polymers.

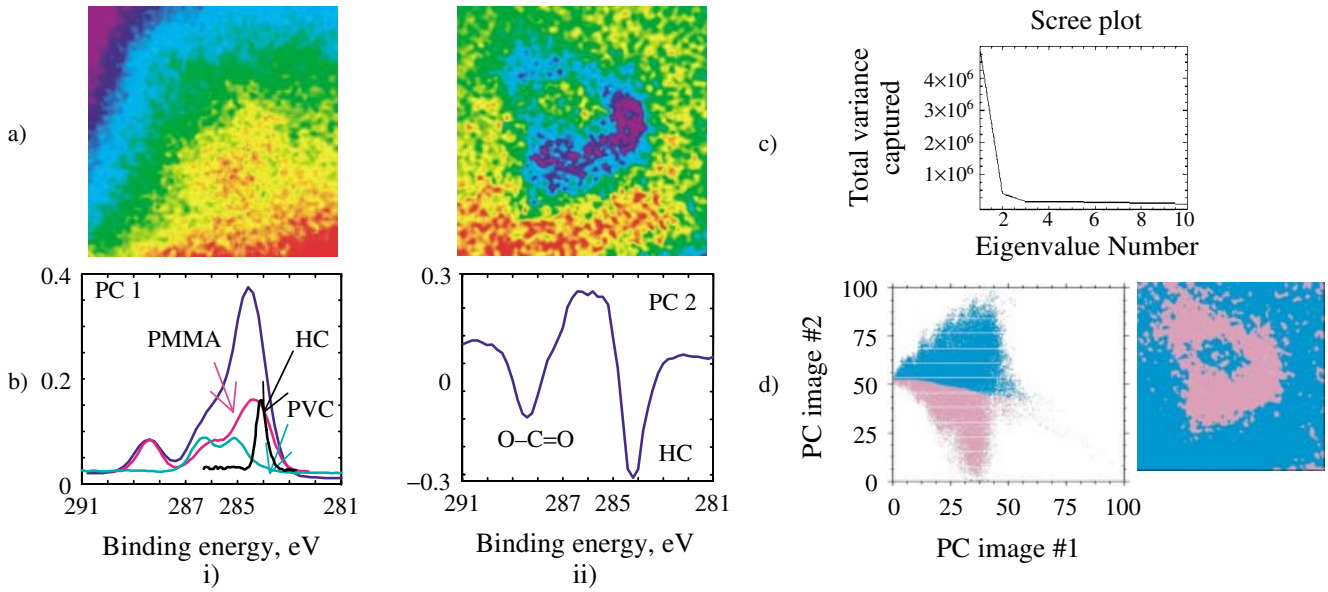

Plate 3. The PCA results applied to the images-to-spectra data set: (a) scores and (b) loadings for first (i) and second (ii) components; (c) scree plot and (d) ICP of first vs. second principal component images. The knee in a scree plot (c) shows a two-component system. The scatter plot of principal component image 1 vs. principal component image 2 is divided into two parts: and back-projected to region of the original image. The phase distribution resembles the Cl 2p image.

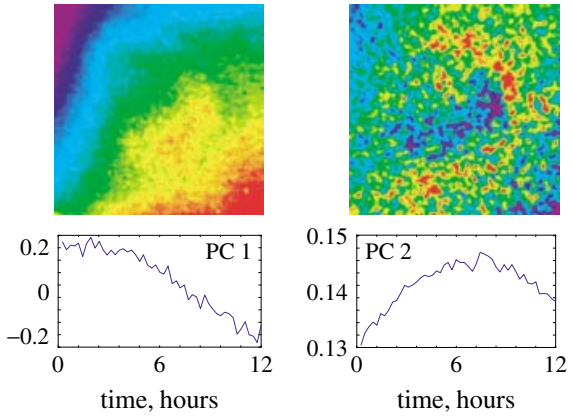

Plate 4. The PCA results applied to the degradation data set: scores and loadings for first and second components.

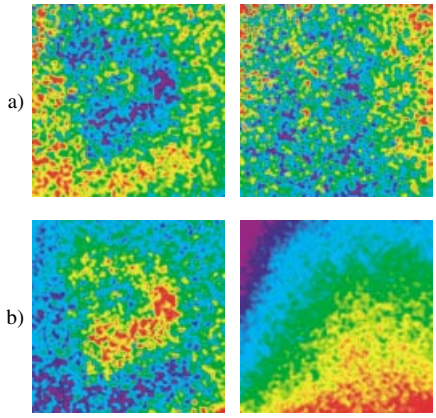

Plate 5. Spectral fitting classification of multispectral data set using Spectral Angle Mapper (a) and Linear Unmixing (b) algorithms. Two phases are shown.

variable images. One of the most important uses of principal components is in scatter plots of one principal component image against another.

Classification

This is the process of assigning data to one of a fixed number of possible classes.[11,19,20] The goal is to convert the numerical image data into descriptive labels that categorize different surface materials or conditions. *Similarity* between pixels or groups of pixels is a fundamental concept behind classification, because the same labels are assigned to areas on the sample that have similar chemical or physical characteristics. Phase maps—images that show the spatial distribution of a particular phase or pixel category—are obtained from classification methods.

Traditionally, thematic classification of an image involves several steps, as shown in Fig. 2:

(1) *Feature extraction* is used to simplify the image series by applying a spatial or spectral transform to a feature image. Examples include selection of a subset of bands, a PCA to reduce the data dimensionality or a spatial smoothing filter. This step is optional.
(2) *Extraction of training pixels* is required to identify the pixels to be used for training the classifier to recognize certain categories of classes. In order to classify an image into specific categories, the classification algorithm needs to be trained to distinguish between those categories. Representative category samples, known as *prototypes*, exemplars or simply *training samples*, are used for this purpose. The *discriminant* function built on the basis of these training regions is used to assign a class label to each pixel.
(3) *Labeling* applies the discriminant function to the entire image and labels all pixels. The rules developed during training are used to assign each pixel in the image to one of the training categories. The output map consists of one label for each pixel.

The training of a classification algorithm can be either *supervised* or *unsupervised*. In supervised classification, the training samples are labeled by the analyst based upon external knowledge. In unsupervised classification, the training pixels are not labeled based upon predetermined phases but are evaluated statistically to identify distinguishing intrinsic data characteristics.

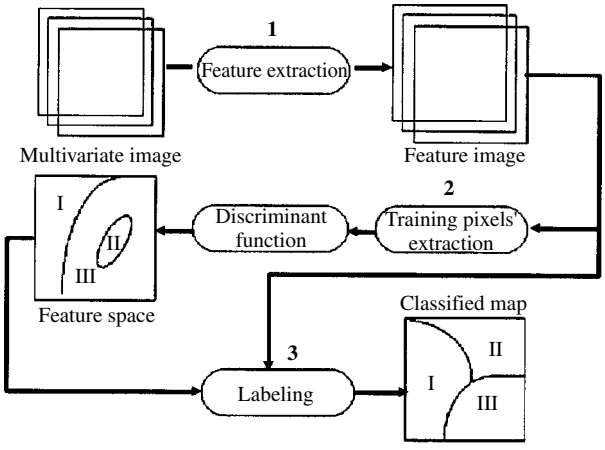

Figure 2. Introduction to the Image Classification algorithm. For step descriptions, refer to the text.

Supervised training. If the multivariate images contain sufficiently distinct visual cues, it may be possible to find suitable training areas by visual examination. Frequently, however, one must resort to additional information to find representative areas for each class. The process of finding and verifying training areas therefore can be rather labor intensive. With supervised training, it is important that the training area be a homogeneous sample of the respective class but at the same time include the range of variability expected for the class. Thus, more than one training area per class often is used.

After selecting the training regions for each class/group in the sample, the location of the point that represents the means for all variables in the multivariate space, called group *centroids*, is determined. Interclass *separability* or *similarity* between pixels is used to assign each pixel to a particular class. Measures of the separation of means include the Euclidean, Mahalanobis and angular distances.[15] The Mahalanobis distance measure is a multivariate generalization of the Euclidean measure for normal distributions. For each pixel the distances of the respective pixel from each of the group centroids are computed. Linkages of groups are then determined based upon the method used to determine association between groups.

Unsupervised classification. This uses statistical techniques to group *n*-dimensional data into their natural spectral classes and does not require training or preconceived notions of pixel classes. This method is based purely on grouping or clustering the data. In defining image areas for unsupervised training, the analyst does not need to be concerned with the homogeneity of the sites. Heterogeneous sites can be chosen deliberately to insure that all classes of interest, as well as within-class variabilities, are included. It is possible also to use the entire image in the clustering algorithm for a 'wall-to-wall' description. The assignment of identifying labels to each cluster may be done by the analyst after training or after classification of the image. For unsupervised training, such as K-means or the Isodata clustering algorithm, the analyst employs an algorithm that locates concentrations of feature vectors within a heterogeneous sample of pixels.[15] These so-called clusters then are assumed to represent classes in the image and are used to calculate class signatures. However, they may or may not correspond to classes of interest to the analyst. Supervised and unsupervised training thus complement each other. In supervised classification, the analyst imposes knowledge on the process to constrain classes and their characteristics, whereas in unsupervised classification an algorithm determines the inherent structure of the data, unconstrained by external knowledge.

A critical question is how well do the class data signatures in the image correspond to the class physical characteristics that actually distinguish one category from another? The spectral signature of a given surface material is not characterized by a single spectral vector, but rather by a distribution of vectors. To a large extent the ability to perform an

accurate classification of a given multivariate image is determined by the extent of overlap between class signatures.[15] The notion of a thematic map presumes that every spot on the material can be labeled as belonging to one, and only one, category. Such discrete categorization is convenient and appealing in its simplicity but is not a particularly accurate portrayal of real surfaces and, in fact, is inconsistent with the high-resolution numerical nature of hyperspectral data. *Non-parametric* algorithms based on such discrete categorizations (similarity-based) make no assumptions about the probability distribution, whereas *parametric* classification algorithms assume a particular statistical class distribution, commonly the normal distributions. Non-parametric methods often are considered robust because they may work well for a wide variety of class distribution, as long as the class signatures are reasonably distinct.

Artificial neural network (ANN) classification is a recently popular non-parametric approach used for non-linear classification.[15,19] It differs significantly from other methods, such as the Mahalanobis distance algorithm, in that the decision boundaries are not fixed by a deterministic rule applied to the prototype training signatures, but are determined in an iterative fashion by minimizing an error criterion on the labeling of the training data. In that sense, ANNs are similar to unsupervised clustering algorithms. A neural network is a system composed of many simple processing elements operating in parallel whose function is determined by network structure, connection strengths and the processing performed at computing elements or nodes. The discrimination ability of an ANN is contained in its inter-unit connection strengths or weights obtained by a process of adaptation to, or learning from, a set of training patterns. During training, they are iteratively adjusted towards a configuration that allows the network to distinguish the prototype patterns of interest. A back-propagation algorithm minimizes the squared error over all patterns at the output of the network.

Parametric algorithms rely on assumptions about the form of the probability distribution for each class and require estimates of the distribution parameter, such as the mean vector and covariance matrix, for classification. The most notable example is Maximum Likelihood, which explicitly uses a probability model to determine the decision boundaries.[15] The necessary parameters for the model are estimated from training data. If a sufficiently large number of representative training pixels are available in each class, the class histograms can be calculated and used as approximations to the continuous probability density functions of an infinite data sample. To make a classification decision for a pixel, it is necessary to know a *posteriori* probabilities that the pixel belongs to each of the training classes, given that the pixel has a feature vector. It is intuitively satisfying to assign the pixel to a particular class if its *a posteriori* probability is greater than that for all other classes; this is the rule for the Maximum Likelihood classifier.

Various spectral fitting algorithms also exist. In these algorithms, external information is the basis for assigning each pixel to a particular phase, utilizing idealized pure signatures for a class (end-member collection).[15,20] As a result of noise and within-class signature variability, end-members exist only as a conceptual convenience and as an idealization in real images.

Mixed pixel classification is the process by which the proportions of the pure components that are present in the part of the image giving rise to the mixed pixel are inferred.[19] The process is otherwise known as 'spectral unmixing'. The basic assumption behind classification using the Linear Spectral Unmixing algorithm is that the spectrum of a mixed pixel has been created by the linear superposition of the spectra of the pure components. The coefficients of the linear superposition are equal to the fraction of the pixel area covered by the corresponding pure components (Fig. 3). Pixels represent a spatial average over some sampling area, therefore it is inevitable that multiple spectral categories will be included in some of them. An increase in spatial resolution may reduce the percentage of mixed pixels, but mixed pixels will still occur at the boundary between objects regardless of spatial resolution. The class fraction determines the location of the mixed-pixel vector in feature space. The inversion problem, termed unmixing, is to estimate the fractions of each class from a given pixel vector.

The Spectral Angle Mapper is a physically-based spectral classification that uses an *n*-dimensional angle to match pixels to end-member spectra.[20] The algorithm determines the spectral similarity between two spectra by calculating the angle between the spectra, treating them as vectors in a space with dimensionality equal to the number of bands. The spectral-angle distance is independent of the magnitude of the spectral vectors and therefore is insensitive to topographic variations.

The Spectral Angle Mapper and Linear Spectral Unmixing classifiers should provide more reliable phase distribution than the supervised classification method, in which the user may influence the outcome of classification by choosing different training regions, thus in some cases 'under'- and in some cases 'over-classifying' the phases at the risk of obtaining unreal phase distributions.

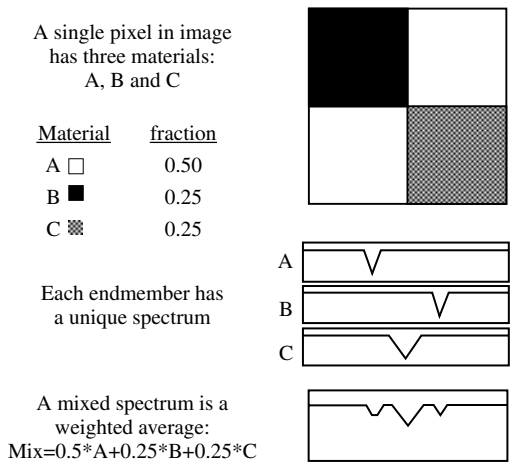

Figure 3. Introduction to Linear Spectral Mixing algorithm.

EXPERIMENTAL

Sample preparation

(Poly(vinyl chloride) (PVC) of molecular weight 77.3 kDa and poly(methyl methacrylate) (PMMA) of molecular weight 100 kDa were obtained from Scientific Polymer Products, Inc. As-received materials were used in 2% w.v. solutions of PVC and PMMA in HPLC-grade tetrahydrofuran (THF). Solutions containing a 50 : 50 mixture of the two polymers were allowed to sit for 24 h before deposition onto teflon watch glasses using pipettes. The resulting films were air-dried for 24–48 h. The films were peeled from the teflon substrate before analysis by XPS. The PVC and PMMA standards were prepared in a similar manner. The air-facing side of the samples was analyzed by XPS.

X-ray photoelectron spectroscopy Instrumentation

The XPS spectra and images were acquired on a Kratos AXIS Ultra photoelectron spectrometer using a monochromatic Al Kα source operating at 300 W. The base pressure was 2×10^{-10} Torr and the operating pressure was 2×10^{-9} Torr. Charge compensation was accomplished using low-energy electrons. Standard operating conditions for good charge compensation are −2.8 V bias voltage, −1.0 V filament voltage and a filament current of 2.1 A.

Data acquisition

In order to evaluate different algorithms for MIA, three XPS data sets were acquired from the same area on the sample. Medium-magnification 350 × 350 μm O 1s, Cl 2p and C 1s images were acquired for 3 min each at a pass energy of 80 eV, producing a bivariate data set of size [256 × 256 × 3].

The images-to-spectra experiment acquires images as a function of binding energy. Medium-magnification images were acquired over the binding energy range of 289–279 eV with a 0.2 eV step. This corresponds to a binding energy range of 291–281 eV after charge correction. A pass energy of 80 eV and an acquisition time of 2 min per image were employed. This experiment creates a multispectral data set, consisting of 50 images, of size [256 × 256 × 50]. In parallel with the images-to-spectra experiment, a C 1s image at a binding energy of 283 eV (285 eV after charge correction) was acquired after each image in the images-to-spectra acquisition. This binding energy corresponds to the peak maximum in the high-resolution C 1s spectrum. This multitemporal degradation image data set is the same size as the multispectral set, using standard conditions of 80 eV pass energy and 2 min acquisition times.

Programs used

All image data files were transferred from the KRATOS format to a format supported by MATLAB[21] and ENVI[22], which is ASCII and a generalized raster data format consisting of a simple 'flat binary file' and a small associated ASCII (text) header file, respectively.

Image analysis was performed using both MATLAB and ENVI. Image processing methods, including scatter diagrams and multivariate image analysis, utilized ENVI. The image PCA routine in the PLS_Toolbox[23] in MATLAB is used to extract spectral or intensity profiles/loadings from images-to-spectra and degradation data, respectively.

Procedure applied

The Cl 2p, O 1s and C 1s photoelectron images are used as references for the evaluation of algorithm performance. The evaluation of the image processing and analysis methods involves several steps. Initially, the Cl 2p, O 1s and C 1s reference images are analyzed using two-dimensional scatter diagrams of different pairs of images in order to find correlations between the images and to identify unique pixels and phases present in the blend.

The MIA methods are tested using the multispectral and multitemporal data sets. The goal is to resolve components, component maps, spectral and intensity profiles and to compare these with chemical XPS images and spectra for identification. First, the number of components present in the data set is determined and component images are extracted in the ENVI PCA routine; then, the corresponding spectral and intensity profiles are resolved in the *imagepca* routine in PLS_Toolbox. The resulting principal component images (scores) and corresponding spectral/intensity profiles (loadings) then are evaluated further. Principal component maps are analyzed individually using scatter plots. Unique correlated and/or anti-correlated clusters in the scatter diagrams can be back-projected to chemical images to identify areas of interest.

Different classification algorithms then are applied to classify chemical phases in the images-to-spectra and degradation data sets. For supervised classification, different training regions are selected and used for evaluation of the performance of two non-parametric algorithms (Mahalanobis Distance and Neural Net) and one parametric algorithm (Maximum Likelihood). An unsupervised K-means classifier using different numbers of classes is applied to the identification of phases in the images without external constraints. High-resolution C 1s spectra of PVC and PMMA are used as reference spectra in the Spectral Angle Mapper and Linear Spectral Unmixing classification methods. The classification produces an approximation to the original image, which allows for evaluation of the classifier on the basis of the accuracy of this approximation. We will use this approach to compare classification results with the original chemical images.

RESULTS AND DISCUSSION

The PVC/PMMA system

Background information

In order to be able to compare information extracted by MIA methods with the knowledge about the PVC/PMMA system, the degradation of PVC under x-ray exposure and the morphology of PVC/PMMA blend should be well understood. Polymer blends containing PVC have been studied extensively by XPS[24–34] as a result of both theoretical and practical interests. A variety of methods have been used to characterize blends containing PVC and PMMA, leading to inconsistencies and conflicting conclusions regarding surface structure.[24,26–28] The inconsistencies are the consequence of

different sampling areas utilized in the various studies, because the level of heterogeneity detected depends upon the analysis area of the characterization technique and the number of areas/film analyzed.

The PVC/PMMA films prepared from THF solutions show heterogenous features that are evident from visual inspection in some cases. Surface analysis of the blends using current XPS instruments with small sampling areas and ToF-SIMS imaging of such films demonstrated heterogeneous surface composition with an enrichment of PMMA at the surface.[25,29,31] Extensive analysis of this polymer blend by a combination of spectroscopy and imaging in our group shows a phase separation of the two polymers on the air side of the films, whereas the substrate side is more homogeneous and mainly contains PVC.[31–34] Scanning electron microscopy analysis revealed bulk phase separation extending to the outermost 1 μm.[28] A comparison of XPS linescans with SEM micrographs of the film suggested either a thin film of PMMA on top of the PVC or smaller PVC domains contained within large PMMA domains.[30] Results obtained by Briggs *et al*. from ToF-SIMS studies also suggested the presence of a thin overlayer of PMMA.[29]

Halogenated compounds, particularly chlorinated ones, are especially sensitive to x-ray exposure, resulting in a decrease in the halogen peak intensity and an increase in the C 1s peak intensity in photoelectron spectra.[12–14] The degradation process probably involves a series of free-radical reactions initiated by both x-ray impact-induced and thermal bond cleavage accompanied by HCl release. The labile chlorine, when cleaved, attacks the methylene protons leading to dehydrochlorination by a free radical mechanism, followed by the formation of conjugated double bonds.[35]

It has been shown that the dehydrochlorination rates of PVC in complex multicomponent polymer samples depend on the method of blending, the solvent used and the affinity of the polymers.[35,36] The PVC/PMMA polymer blend system phase separates with the formation of two phases: one enriched in PVC and the second enriched in PMMA, although both PMMA and PVC are present in each phase. The rate of degradation of PVC, thus, potentially will be affected by the presence of PMMA.

This extensive prior characterization makes the data a suitable test case for the evaluation of MIA methods.

Original data sets

The Cl 2p, O 1s and C 1s images acquired from the same area on the sample are shown in Plate 2. The Cl 2p image, in which bright areas are enriched in PVC, shows the highest contrast, and contains a large circular feature in the center of the image. The O 1s image, in which the bright areas are enriched in PMMA, has lower contrast but still shows a good anti-correlation with the Cl 2p image. The C 1s image, to which both polymers contribute approximately equally, is the most featureless and the spatial distribution of phases is not clear.

Selected images from the multispectral and multitemporal data sets are shown in Fig. 4(a) and 4(b), respectively. The images-to-spectra data set consists of images acquired over the energy range of 291–281 eV in 0.2 eV steps, whereas

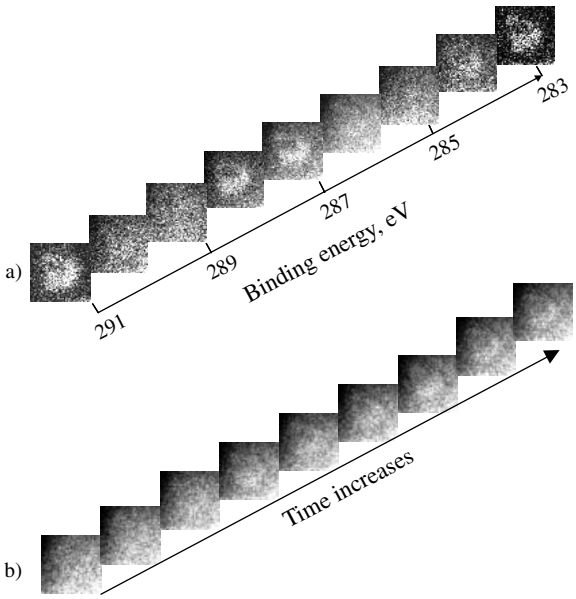

Figure 4. (a) Multispectral data from the images-to-spectra experiment. Note that images at different binding energies possess different spatial information. (b) Multitemporal C 1s data from degradation experiment. Note that all images within the data set are featureless.

the degradation data set consists of 50 images acquired at the same binding energy (285 eV). In the multispectral image data set, images are acquired over the binding energy range corresponding to the high-resolution C 1s spectrum. The high-resolution C 1s spectrum is a convolution of overlapping peaks from PVC and PMMA. Representative C 1s degradation spectra for the pure polymers are shown in Fig. 5. The PMMA has a distinct peak where there is no signal from PVC around 289 eV due to the O–C═O bond, whereas PVC has a distinct peak at 287 eV that is the C–Cl component of PVC. This separation of chemical features within the C 1s binding energy range means that images at some energies in the images-to-spectra experiment will have a dominant contribution from one of the polymers and therefore will possess spatial information related to the distribution of this polymer. Indeed, some of the images in Fig. 4(a) show a feature similar to that in the Cl 2p image, which is representative of PVC. The images-to-spectra data set is thus used for the initial evaluation of the performance of MIA methods.

The multitemporal data set consists of a series of images acquired at the constant binding energy of 285 eV, at which both polymers contribute equally, resulting in a featureless image with no spatial structure [Fig. 4(b)]. This data set thus provides a more difficult analysis problem than the multispectral data set.

Bivariate image analysis

Scatter plots for C 1s vs. O 1s, C 1s vs. Cl 2p and Cl 2p vs. O 1s images are shown in Fig. 6(i). The first scatter plot has a cluster of points concentrated along the first diagonal, indicating a high degree of correlation between the C 1s and O 1s images (Plate 2). Indeed, the C 1s and O 1s images are different only in the central portion of the

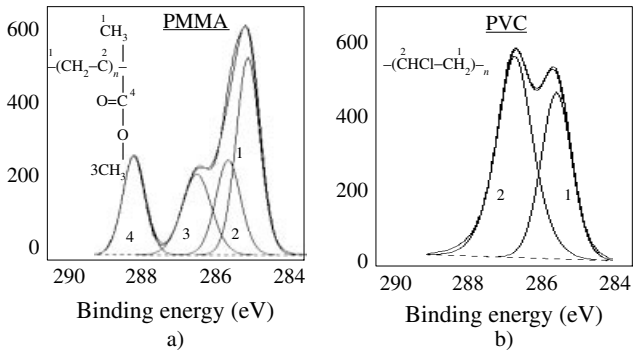

Figure 5. High-resolution C 1s spectra from pure PMMA (a) and pure PVC (b). These spectra are used as a reference for Spectral Fitting Classification algorithm.

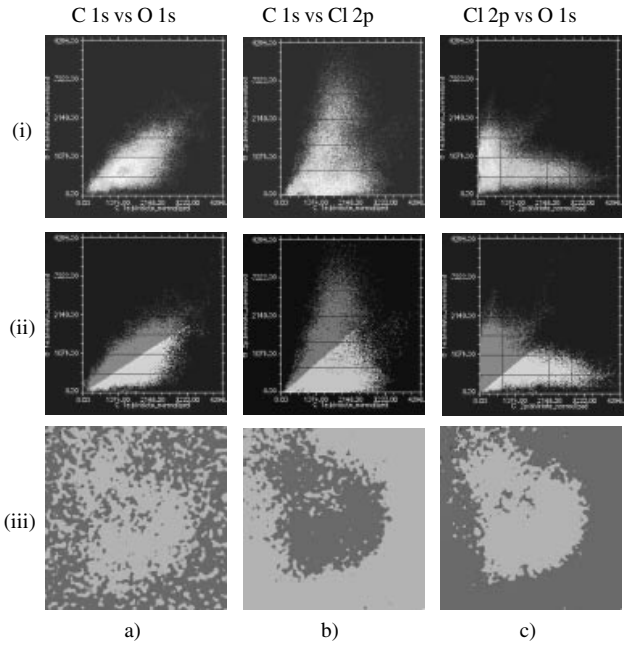

Figure 6. Bivariate analysis. (i) scatter plot of photoelectron images, (ii) scatter plot divided into two regions by first diagonal and (iii) back-projected regions to original image for (a) C 1s vs. O 1s,(b) C 1s vs. Cl 2p and (c) Cl 2p vs. O 1s.

images, corresponding to the bright PVC-enriched feature in the Cl 2p image. The scatter plot for C 1s vs. Cl 2p images is more disperse, indicating less correlation between these images. Thus, the PMMA distribution (O 1s image) has a higher correlation with the blend distribution C 1s image) than the PVC distribution (Cl 2p image) does. In other words, within the C 1s image of the blend there are areas where there is essentially no PVC, whereas most areas in the image have a contribution from PMMA. This points towards the existence of a PMMA overlayer, as was concluded previously by different groups, including ours, using multiple techniques.[25,29–32] The third scatter plot of Cl 2p vs. O 1s also shows a significant spread in the data without any particular trend.

To understand better the phase distribution, ICP can be utilized. Initially, all of the scatter plots are divided into two parts by the first diagonal, as shown in Fig. 6(ii). The parts of the image contributing to specific areas in the scatter plots are determined by back-projecting these two parts of the cluster to the original image. In this example, two phases are distinguished: one corresponding to the bright circular feature in the Cl 2p image and a second corresponding to the bright area on the O 1s image [Fig. 6(iii)]. There is no distinct interface between the two phases obtained from the first scatter plot C 1s vs. O 1s in Fig. 6(iii-a). This is probably because the O 1s signal from PMMA and the C 1s signal from both polymers are highly correlated as a result of the PMMA overlayer. The other two scatter plots produce high contrast phase maps, resembling the Cl 2p image overlaid with the O 1s image.

The ICP is an interactive process in which the user decides how to divide the scatter diagram into parts. A different example is shown in Fig. 7(i). In this case, the Cl 2p vs. O 1s scatter plot is divided into three parts by two lines parallel to the first diagonal (the direction of highest correlation). This division results in three back-projected phases. The region of highest correlation between the two images is concentrated along the first diagonal (darkest part on the scatter diagram), corresponding to the intermediate region between two other phases. This region can be identified as a 50 : 50 blend, because O (PMMA) and Cl (PVC) contribute equally to the intensity in this region. The cluster to the right of the central region on the scatter diagram corresponds to the part of the image in which the signal from O 1s is low, whereas the signal from Cl 2p is high. This region thus represents a PVC-enriched area, similar to the circular region on the Cl 2p image. The cluster to the left of the central diagonals represents the region enriched in PMMA. External knowledge of the sample structure, available directly from the XPS images, was obviously helpful in the attribution of a particular part of the scatter diagram to a specific phase. It is worth noting that although the ICP method is a somewhat subjective procedure, variation in the method of dividing the scatter diagram into three parts caused only minor changes in the intermediate region between the two phases, while the overall spatial structure was not affected [Fig. 7(b)].

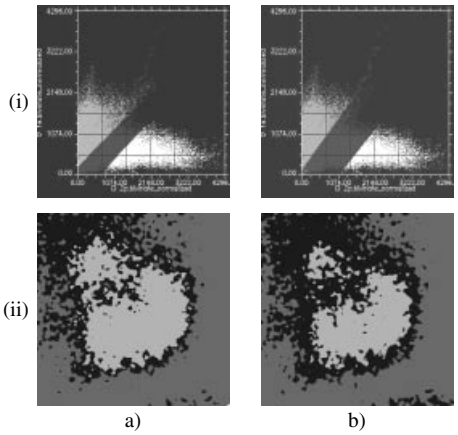

Figure 7. Bivariate analysis: (a) and (b) represent two different divisions of the scatter plot of Cl 2p and O 1s images (i) and back-projected regions to the original image (ii). Although the distribution of phases is slightly changed, the overall spatial structure is the same from both divisions.

Multivariate image analysis

Applying PCA to the multispectral images-to-spectra data set results in component maps (scores) and corresponding spectral profiles (loadings), as shown in Plates 3(a) and 3(b). Two principal components are determined to be present in the system. This conclusion is based upon the location of the knee in the scree plot [Plate 3(c)], which is a plot of total variance captured by the eigenvalues versus the number of the eigenvalue.

It is possible to identify components based on the visual inspection of principal component images. For this purpose we use elemental C 1s, O 1s and Cl 2p photoelectron images (Plate 2) as the reference for comparison. The principal component map of the first component is similar to the C 1s image acquired at 285 eV [Plate 2(a)], in which peaks from both polymers overlap. There is also a pronounced feature in the map of the first component that is similar to the PVC-enriched area in the center of the Cl 2p image [Plate 2(c)]. This images-to-spectra experiment takes ~12 h to acquire. During this time PVC degrades through a dehydrochlorination mechanism. The product of PVC degradation—hydrocarbon (HC)—will contribute to the intensity and photopeak shape of the C 1s peak. In C 1s images, therefore, the HC contribution will be most pronounced in the areas enriched with PVC, which is the bright circular feature in the Cl 2p image. Based on this comparison, the first extracted component can be identified as resulting from the 50 : 50 blend after pronounced PVC degradation. The map of the second extracted component is similar to the O 1s image [Plate 2(b)] or an inverse of the Cl 2p image. Identification of this component based only on principal component image appearance is not possible.

A scatter diagram for the two principal component images is shown in Plate 3(d). Interactive correlative partitioning by division of the scatter diagram into two clusters, followed by back-projection to the original image, results in a more readily interpretable image. Plate 3(d) shows the spatial distribution of two phases present in the blend, one phase enriched in PVC and a second phase enriched in PMMA.

The spectral profiles (loadings) extracted by PCA [Plate 3(b)] allow for the identification of both components based upon a comparison of component shapes to the high-resolution C 1s spectra of the pure polymers as shown in Fig. 5. The shape of the first extracted loading is similar to the C 1s spectrum of the blend with a high HC content from degradation. This result is in good agreement with the identification of the first component from the principal component image inspection. The loading of the second component is negative with respect to the baseline peaks, and a chemical identification is not justified. Mathematically, however, two peaks are observed in the second spectral profile at ~284 eV and ~288.5 eV, which can be attributed to HC as a product of PVC degradation and O–C═O from PMMA, respectively. The contribution from PMMA to the second loading may explain the similarity of the second component image to the O 1s image. An unexpected correlation between a product of PVC dehydrochlorination (HC) and the O 1s signal from PMMA is thus observed. The authors initially expected that a component representative only of the HC would be extracted by PCA, because the degradation product concentration increases with x-ray exposure time.

Visual analysis of the C 1s degradation data set [Fig. 4(b)] shows very few features in the image series. Plate 4 shows the two components determined by PCA. The extracted maps are very similar to those extracted from the images-to-spectra set [Plate 3(a)]; the only significant difference is the decreased contrast in the map of the second component extracted from the degradation data set. It is possible, based on the PCA analysis, to elucidate the existence of phase-separated regions from the set of images acquired at a constant binding energy without any additional information or experiments. The loadings show component contribution as a function of time. The decrease of the first component with time correlates with the polymer blend degradation, confirming the identification of the first component as a degraded 50 : 50 blend. The increase of the second component confirms identification of the second component as a degradation product, because the signal from HC increases with time.

Although the PVC/PMMA blend was chosen as a well-studied and understood system, the PCA applied to the XPS image series indicates that the degradation behavior of PVC within the blend is more complex than was expected. The product of PVC degradation within a blend is HC correlated with oxygen-containing moieties of PMMA. Confirmation of this result was obtained by MVA of degradation spectral data; a more detailed discussion of the PVC/PMMA blend degradation is presented elsewhere.[36,37] It is apparent that without application of MVA to the spectra and images, some aspects of the degradation behavior of PVC in the polymer blend would be readily overlooked.

Classification

Different classification algorithms are applied to both the degradation and images-to-spectra data sets. It is most appealing to obtain phase information from the C 1s degradation set [Fig. 4(b)] because this series of featureless images does not contain any spatial information, contrary to the images in the images-to-spectra experiment [Fig. 4(a)] that possess significant spatial distribution information. Supervised and unsupervised classification methods were tested using the multispectral (images-to-spectra) and multitemporal (degradation) data sets.

For supervised classification, two regions—representing phases enriched in PVC and in PMMA—were defined for the multispectral and multitemporal data sets. As discussed previously, in order to find the area best representing each class, multiple areas per class should be selected. Several rectangular areas were chosen from bright and dark areas on the second principal component image to represent the two classes or phases [Fig. 8(a)].

In Figs 8(b)–(d) the first two images are phase maps, which show the distribution of pixels assigned to each of the two specified classes. The third image in each set is a composition map, which is an overlay of the two phase maps. The phase and composition maps extracted from the multispectral data set by Mahalanobis Distance, Maximum Likelihood and Neural Net algorithms are shown. All three algorithms utilized the training regions marked in

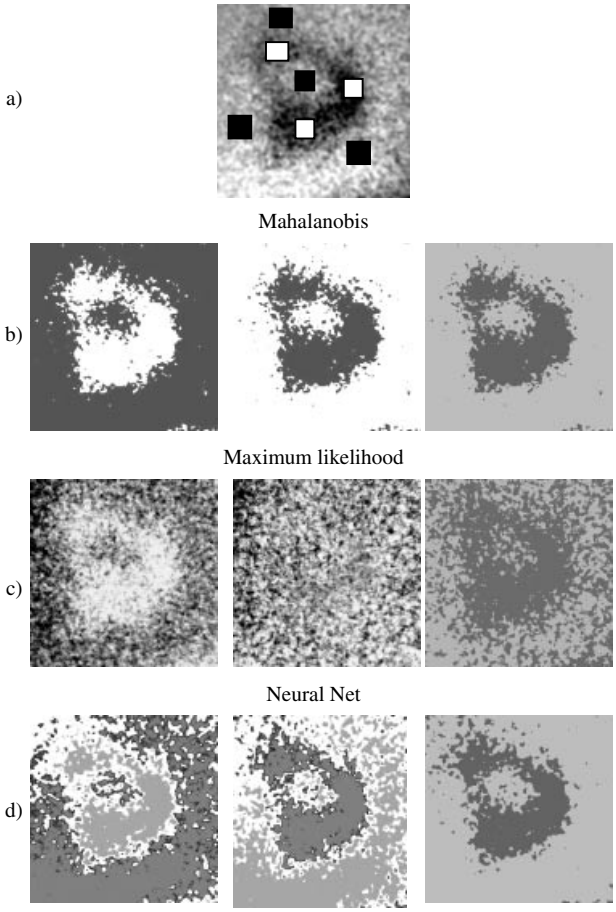

Figure 8. Supervised classification applied to multispectral data set. (a) Training regions selected. Maps of two phases and compositional maps are shown for Mahalanobis Distance (b), Maximum Likelihood (c) and Neural Net (d) algorithms.

Fig. 8(a) and provide compositional maps from which the spatial structure of the polymer blend can be discerned. The Mahalanobis Distance and Neural Net methods gave almost identical results, classifying two phases that are inverses. Phase image 1 is similar in both size and shape to the Cl 2p image and can be identified as a PVC-enriched phase. The second phase, however, cannot be identified as a PMMA-enriched phase in the blend because it is not entirely similar to the O 1s image. In the PVC/PMMA system, the polymers form phases enriched in PVC or PMMA rather than the pure components. The discrete categorization of each pixel that results from non-parametric classification is thus an approximation of the real surfaces, in which overlap between the two phases is present.

The Maximum Likelihood algorithm is a parametric algorithm. It results in a compositional map with less contrast than those generated from the non-parametric algorithms. As shown in Fig 8(c), the first phase image is similar to the Cl 2p image, although the central feature has less distinct edges. The PVC-enriched area thus occupies a larger portion of the image field than in the Cl 2p image (Plate 2). The second phase is a more homogeneous, featureless image that is similar to the C 1s image.

The performance of all supervised classification methods depends very strongly on the training regions selected. Slight deviations from the selected regions cause poor classification. To achieve successful classification, the user must find the training set that best represents the phases. Figure 9 has results from a Mahalanobis classification using three different sets of training regions. The first set is the one used for classification in Fig. 8, the second set is a different selection of multiple rectangular areas representing PMMA and PVC-enriched phases and the third set consists of two areas obtained by back-projecting the areas of highest correlation between the first and second principal components on the scatter plot (Fig. 9 insert) to the original image. The second set of training regions gives results [Fig. 9(b)] similar to the first [Fig. 9(a)], whereas the third training region results in poor classification [Fig. 9(c)]. If there is considerable within-class variability, the selection of training sites can be laborious and it is impossible to be entirely certain that a comprehensive set of training samples for each class has been specified. For many data sets it is impossible to obtain homogeneous training sites.

Composition maps extracted from the multitemporal degradation data set by the same three algorithms (Fig. 10) do not show the same distinct phases as those developed from the images-to-spectra experiment. The Maximum Likelihood and Mahalanobis Distance algorithms perform similarly in this example. The composition map is similar to the last C 1s image in the degradation data set, where the feature resembling the Cl 2p image is most obvious. Applying the Neural Net algorithm to the degradation data set fails to identifying spatial phase distributions, which may be due to the fact that it did not reach a global minimum.

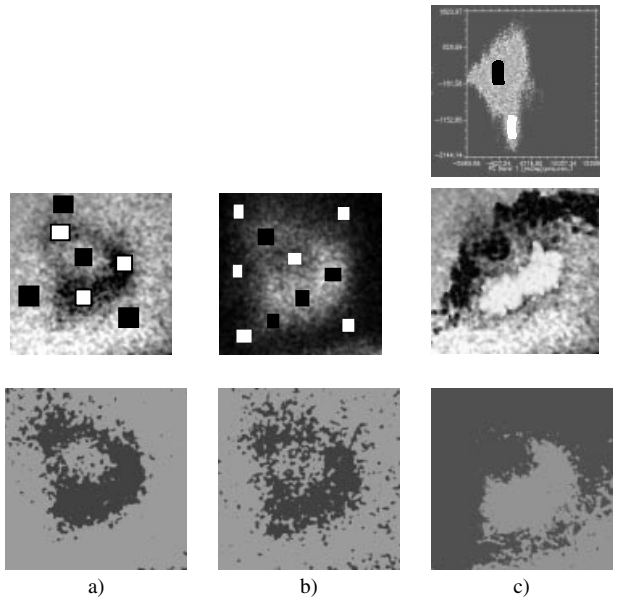

Figure 9. Influence of training regions selected on Mahalanobis Distance classification performance. Three sets of regions are compared: (a) set of multiple rectangular areas (used in Fig. 8); (b) different selection of rectangular areas; (c) two regions back-projected from areas of highest density in the scatter plot of PC1 vs. PC2 (insert). Middle row, training regions, lower row, compositional map classified. The results show that supervised classification is sensitive to training region selection.

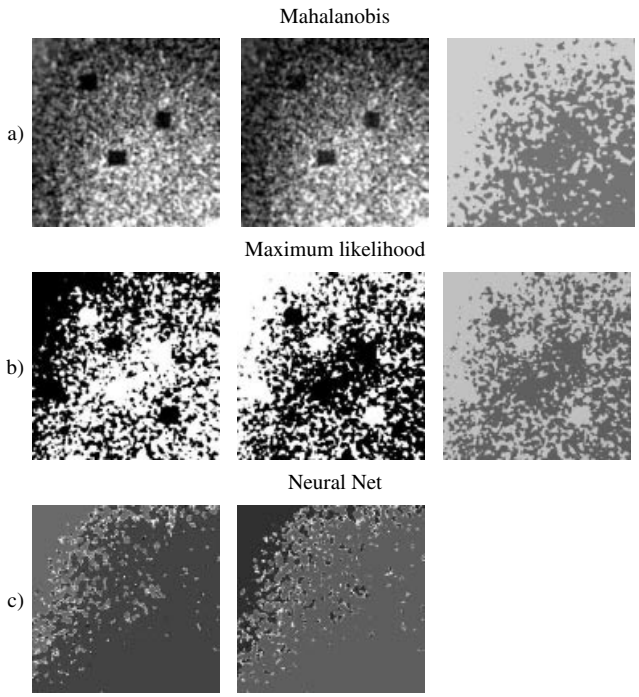

Figure 10. Supervised classification applied to multitemporal data set. Maps of two phases and compositional maps are shown for Mahalanobis Distance (a), Maximum Likelihood (b) and Neural Net (c) algorithms.

Both image data sets were analyzed also using unsupervised classification algorithms. For the unsupervised K-means classifier, two and three classes were selected to be identified in the data sets using the default parameters of the algorithm. Phase maps extracted from both data sets, using two- and three-phase classification, are shown in Fig. 11. The phase maps are virtually identical, with slightly sharper interfaces between phases for the images-to-spectra data set. This algorithm does not result in composition maps that can be compared with the chemical images. At best, part of the circular feature observed in the Cl 2p image is recovered using a three-phase classification.

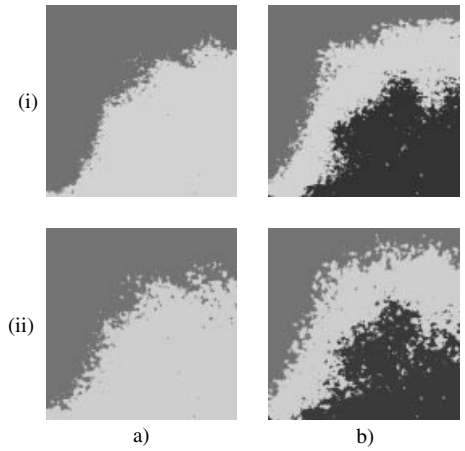

Figure 11. Unsupervised K-means classification of (i) multispectral and (ii) multitemporal data sets using two (a) and three (b) classes.

Spectral-fitting algorithms also can be used to classify the images in the images-to-spectra data set. The Spectral Angle Mapper and Linear Spectra Unmixing algorithms classify pixels in the multispectral data set using reference spectra of pure PVC and PMMA (Fig. 5). The Spectral Angle Mapper classifier compares the spectral profiles of pure components—provided by the user—with the spectrum for each pixel. The pixel then is assigned to one or another class based on the best match. A Spectral Angle Mapper classification using the PVC spectrum as the reference spectrum resolves an image resembling the inverse of the Cl 2p image, whereas using PMMA as the reference results in a homogeneous image with no contrast [Plate 5(a)]. Application of the Linear Spectral Unmixing classifier using the same two reference spectra results in two phases: one resembles the Cl 2p image and the second is similar to the C 1s image. From this classification it can be concluded that the first phase corresponds to PVC degradation within the blend, whereas the second phase represents the blend [Plate 5(b)]. Results obtained from both spectral and multivariate image analysis thus result in the same two components.[34] Spectral fitting methods show obvious advantages over the supervised or unsupervised algorithm because they use external chemical knowledge about the system in study and results are less dependent on user interaction with the algorithm. Unfortunately spectral signatures of pure compounds may not always be available.

CONCLUSIONS

In this study, the goal was the evaluation of different MIA algorithms that can be applied to XPS imaging data sets in order to discover and identify the number of species existing in a multicomponent system and to extract morphological information. The performance of multivariate methods was tested by comparing the extracted information with the chemical information from the PVC/PMMA polymer blend.

Scatter diagrams provide a rapid analysis of the image content in terms of correlation and anti-correlation. Interactive correlation partitioning allows for a rapid determination of the spatial relation of pixels possessing a chemical similarity to be studied, thus identifying phases.

Principal component analysis applied to the multispectral data set allows for the identification of both components based upon the principal component image and loading shape: the first component is the blend after degradation and the second component is a degradation product (HC correlated with the O–C═O part of PMMA). It is possible, based on the PCA analysis of the multitemporal image data, to elucidate the existence of phase-separated regions without any additional information or experiments.

Supervised classification methods work well for classification of the two phases in the images-to-spectra data set. The two phases classified by non-parametric methods are inverses, as a result of the discrete categorization of each pixel into one of the classes. In the case of the polymer blend system, though, the polymers separate into phases enriched with one or another component and not into the pure polymer phases. The Maximum Likelihood algorithm,

which relies on assumptions about the form of the probability distribution for each class, results in a more chemically reasonable solution than non-parametric algorithms.

Composition maps extracted from the multitemporal degradation data set by the same three algorithms are not as well-defined as those developed from the images-to-spectra experiment. The Neural Net applied to the degradation data set fails in identifying spatial phase distributions, which is probably due to the fact that it did not reach a global minimum.

The sensitivity and subjectivity of supervised methods to training region selection are demonstrated. Slight deviations from the selected regions cause poor classification. To achieve successful classification, the user must find the training set that best represents the phases and variations in values.

Unsupervised classification does a poorer job in classifying phases for both data sets. Only the part of the central circular feature responsible for the enriched PVC area in the blend image is identified, and the total spatial representation of phases within the image is not clear.

The spectral fitting methods show obvious advantages over the supervised and unsupervised algorithm, because they use real external chemical knowledge about the system and are less dependent on user interaction with the algorithm. Correlating these results to those obtained from PCA, where one component is from the blend and another is a product of degradation, phases resembling the blend and product of PVC degradation (which is an HC correlating with the oxygen signal from PMMA) are identified.

The PVC/PMMA blend was initially chosen as a test system for the evaluation of various algorithms because the authors considered it to be a well-studied system. Multivariate image analysis techniques applied to the XPS images indicate that the degradation behavior of PVC within the blend is more complex than was expected. This study thus also demonstrates that the appropriate application of surface chemometrics can extract 'hidden' information from complex data.

Acknowledgements

This work has been partially supported by NSF ALCOM (DMR89-20147). The XPS was funded by a grant from the Keck Foundation and by NSF CHE-9613880.

REFERENCES

1. Prutton M, Wilkinson DK, Kenny PG, Mountain DL. *Appl. Surf. Sci.* 1999; **145**: 1.
2. Bonne N. *Mikrochim. Acta* 1999; **120**: 195.
3. Browning R. *Surf. Interface. Anal.* 1993; **20**: 495.
4. Kaufmann K, Baumeister W. *Z. Angew. Math Mech.* 1996; **76**: 467.
5. Saurina J, Hernandez-Cassou S. *Analyst* 1999; **124**: 745.
6. de Juan A, Rutan SC, Tauler R, Massart DL. *Chemometr. Intell. Lab.* 1998; **40**: 19.
7. Centner V, Verdu-Andres J, Walczak B, Jouan-Rimbaud D, Despagne F, Pasti L, Poppi R, Massart DL, de Noord OE. *Appl. Spectrosc.* 2000; **54**: 608.
8. Prutton M, Barkshire IR, Kenny PG, Roberts RG, Wenham M. *Philos. Trans. R. Soc. A* 1996; **354**: 2683.
9. Barkshire IR, Kenny PG, Fletcher IW, Prutton M. *Ultramicroscopy* 1996; **63**: 193.
10. Hutter H, Grasserbauer M. *Chemometr. Intell. Lab.* 1994; **24**: 99.
11. Stubbings TC, Wolkenstein MG, Hutter H. *J. Trop. Microp. Tech.* 1999; **17**: 1.
12. Duca MD, Plosceanu CL, Pop T. *J. Appl. Polym. Sci.* 1998; **67**: 2125.
13. Pesin LA, Baitinger EM, Kudryavtsev YP, Evsyukov SE. *Appl. Phys. A-Mater.* 1998; **66**: 469.
14. Vointseva II, Gilman LM, Kudryavtsev YP, Evsyukov SE, Pesin LA, Gribov IV, Moskvina NA, Khvostov VV. *Eur. Polym. J.* 1996; **32**: 61.
15. Richards JA, Jia X. *Remote Sensing Digital Image Analysis: an Introduction*. Springer: Berlin, New York, 1999.
16. Prutton M, Elgomati MM, Kenny PG. *J. Electron Spectrosc. Relat. Phenom.* 1990; **52**: 197.
17. Geladi P, Hans G. *Multivariate Image Analysis*. John Wiley: Chichester, 1996.
18. Geladi P, Isaksson H, Lindquist L, Wold S, Esbensen K. *Chemometr. Intell. Lab.* 1989; **5**: 209.
19. Chang CI, Ren H. *IEEE Trans. Geosci. Remote* 2000; **38**: 1044.
20. Chang CI. *IEEE Trans. Inform. Theory* 2000; **46**: 1927.
21. *MATLAB: The Language of Technical Computing*. The Mathworks: Natick, MA, version 12.1.
22. *ENVI: The Environment for Visualizing Images*. The Research Systems: Boulder, CO, version 3.1.
23. *PLS_Toolbox 2.0*. Eigenvector Research: Manson, WA.
24. Schmidt JJ Jr, Gardella JA, Salvati L. *Macromolecules* 1989; **22**: 4489.
25. Burkhardt CA Jr, Gardella JA. *Appl. Spectrosc.* 1993; **47**: 1636.
26. Short RD, Ameen AP, Jackson ST, Pawson DJ, O'Toole L, Ward AJ. *Vacuum* 1993; **44**: 1143.
27. Briggs D, Fletcher IW, Reichmaier S, Agoulo-Sanchez JL, Short RD. *Surf. Interface Anal.* 1996; **24**: 419.
28. Jackson ST, Short RD. *J. Mater. Chem.* 1992; **2**: 259.
29. Leeson AM, Alexander MR, Short RD, Briggs D, Hearn MJ. *Surf. Interface Anal.* 1997; **25**: 261.
30. Jackson ST. PhD. Thesis, University of Sheffield, UK, 1982.
31. Thomas EA, Fulghum JE. *J. Vac. Sci. Technol. A* 1998; **16**: 1106.
32. Artyushkova K, Wall B, Koenig J, Fulghum JE. *Appl. Spectrosc.* 2000; **54**: 1549.
33. Artyushkova K, Fulghum JE. *Surf. Interface Anal.* 2001; **31**: 352.
34. Artyushkova K, Fulghum JE. *J. Electron Spectrosc. Relat. Phenom.* 2001; **121**: 33.
35. Lizymol PP, Thomas S, Jayabalan M. *Polym. Int.* 1997; **44**: 23.
36. Kulish EI, Kolesov SV, Kovarskii AL, Minsker KS. *Vysokomol. Soedin.* 1998; **40**: 267.
37. Kolesov SV, Kulish EI, Minsker KS. *Vysokomol. Soedin.* 1995; **37**: 1084.